COMMUNICATIONS IN COMPUTATIONAL PHYSICS
Vol. **6**, No. 4, pp. 848-882

Commun. Comput. Phys.
October 2009

On a Shallow Water Model for the Simulation of Turbidity Currents

T. Morales de Luna[1,*], M. J. Castro Díaz[1], C. Parés Madroñal[1] and E. D. Fernández Nieto[2]

[1] *Análisis Matemático, Facultad de Ciencias – Univ. Málaga, Campus de Teatinos, s/n, 29071-Málaga, Spain.*
[2] *Dpto. Matemática Aplicada I, ETS Arquitectura – Univ. Sevilla, Avda. Reina Mercedes N. 2, 41012-Sevilla, Spain.*

Received 18 July 2008; Accepted (in revised version) 15 January 2009

Available online 12 March 2009

Abstract. We present a model for hyperpycnal plumes or turbidity currents that takes into account the interaction between the turbidity current and the bottom, considering deposition and erosion effects as well as solid transport of particles at the bed load due to the current. Water entrainment from the ambient water in which the turbidity current plunges is also considered. Motion of ambient water is neglected and the rigid lid assumption is considered. The model is obtained as a depth-average system of equations under the shallow water hypothesis describing the balance of fluid mass, sediment mass and mean flow. The character of the system is analyzed and numerical simulations are carried out using finite volume schemes and path-conservative Roe schemes.

AMS subject classifications: 74S10, 35L60, 35L65, 74G15

Key words: Turbidity currents, hyperbolic systems, finite volume methods, path-conservative schemes, numerical modeling.

1 Introduction

When a river contains an elevated concentration of suspended sediment, to the extent that the river density is greater than that of the receiving water body, the river can plunge and create a hyperpycnal plume or turbidity current. This hyperpycnal plume can travel significant distances until it loses its identity by entraining surrounding ambient water and dropping its sediment load. A sketch of a turbid underflow is presented in Fig. 1.

*Corresponding author. *Email addresses:* morales@anamat.cie.uma.es (T. Morales), castro@anamat.cie.uma.es (M. J. Castro), pares@anamat.cie.uma.es (C. Parés), edofer@us.es (E. D. Fernández)

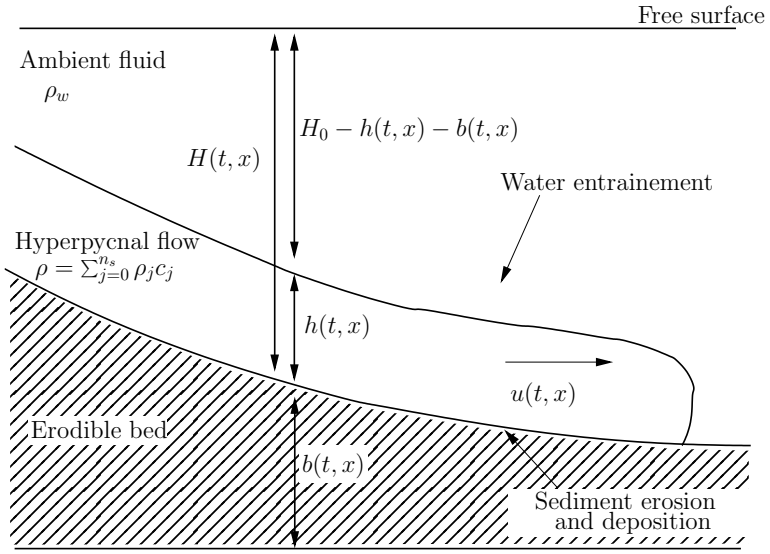

Figure 1: Sketch of hyperpycnal flow.

There is great interest in turbidity currents because of their profound impact on the morphology of the continental shelves and ocean basins of the world. It is commonly accepted that they are one of the potential processes through which sediments can be transferred to the deep sea environments. These bottom currents influence the sea bed morphology by depositing, eroding and dispersing large quantities of sediment particles. The resultant deposit often form porous layer of rocks which are potential sources of hydrocarbon. Therefore, understanding and predicting the geometry of these deposits is crucial for effectively exploring and exploiting these reservoirs.

An additional concern is the destructive effect that turbidity currents have on underwater structures, such as cables, pipelines and foundations.

Large-scale hyperpycnal flow or turbidity currents in the natural environment are difficult to monitor because of the unpredictable nature of the events. As a result, most of our knowledge about these flows is derived from small scale laboratory experiments like the ones described in [1, 12, 17, 18, 20].

Some layer-averaged models have been previously developed on the basis of small-scale tank experiments of particle-driven density currents in [6, 9, 16–18, 24]. The partial differential equation (PDE) system of these models share a common structure, but different parametrization of the relevant mechanisms (deposition, erosion, water entrainment, etc.).

The first goal of this article is to improve this PDE system of the averaged models in order to include some missing effects that we consider to be relevant. More precisely:

1. in the absence of water entrainment, the freshwater mass in the turbidity current should be preserved;

2. the deposition, erosion, and water entrainment should have an effect in the momentum equation;
3. the density of the ambient fluid should be taken into account so that the model could simulate a plume that plunges into the ocean as well as a current flowing in the atmosphere;
4. besides the deposition and erosion fluxes, the sediment transport of bed-load particles may be relevant and therefore it should be included in the model.

To modify the system in order to include the effects 1 to 3, we re-derive the averaged-layer model, as it was done in [24] from the Navier-Stokes equations. The model is obtained by assuming the Boussinesq approximation, the rigid-lid assumption for the ambient flow, and the shallow water hypothesis. Then, the equations are integrated along the vertical direction. In this re-derivation, we are specially careful with the terms corresponding to these missing effects.

For concerns of the missing effect 4, we include a new equation for the thickness of the sedimentary layers. This equation is a standard model for the sediment bed-load transport. In particular, Grass model is considered here (see [14]).

We emphasize the fact that the only improvements proposed here concern the expression of the PDE system, but not the parametrization of the deposition, erosion and water entrainment terms: we just choose some of the most frequently used expressions used for these terms described in the literature. There is surely an interesting work to be done concerning the rigorous justification and/or redefinition of these parametrizations based on the mathematical analysis, but this is a difficult task which is far beyond the scope of this article.

Once the PDE system has been derived, we analyze its mathematical structure. On the one hand, we study its hyperbolic nature, and on the other hand, we investigate the possibility of obtaining an entropy pair. The existence of such a pair is often considered a test for the physical consistency of the model (see [3–5]).

The obtained PDE system has the form of a system of conservation laws with source terms and non-conservative products. The second goal of this article is to propose an adequate finite volume numerical scheme for this system. We propose a generalized Roe scheme of the family introduced in [25]. These schemes are path-conservative in the sense of [22] which implies that the numerical scheme reduces to a conservative scheme for the equations of the system having the form of a pure conservation law.

The organization of this paper is as follows: In Section 2 we describe the model presented here and in particular the empirical relations and physical constants taken into account. In Section 3 the model is obtained from the two dimensional equations under the shallow water hypothesis and hydrostatic distribution of pressure. The character of the system as well as its eigenstructure is studied in Section 4. An entropy inequality is also obtain under some hypothesis. The theory presented in [23] and [22] is adapted in Section 5 in order to define a Roe scheme for the model considered here. Finally, numerical results and comparisons to experimental data are shown in Section 7.

2 Model description

Layer-averaged models have been widely used in the simulation of turbidity currents (e.g., [6, 9, 16–18, 24]). In the framework proposed by these authors, $n_s \geq 1$ species of sediments are considered with constant density ρ_j, for $j=1,\cdots,n_s$. These sediment species are transported by a river with freshwater of constant density ρ_0. The river plunges into an ambient fluid (in general the ocean) of density ρ_w generating a turbidity current. The models presented by the cited authors may be written under the following general formulation:

$$\begin{cases} \partial_t h+\partial_x(hu)=\phi_\eta, \\ \partial_t(hu)+\partial_x\left(hu^2+gR_c\dfrac{h^2}{2}\right)=g(R_0+R_c)h\partial_x H+\tau, \\ \partial_t(hc_j)+\partial_x(huc_j)=\phi_b^j, \text{ for } j=1,\cdots,n_s \\ \partial_t H=\xi\phi_b, \end{cases} \tag{2.1}$$

where h is the current thickness; u is the depth-averaged velocity; c_j for $j=1,\cdots,n_s$ represents the vertically averaged volume concentration of the jth sediment; and H is the bottom depth from a fixed level. Finally,

$$R_j=\frac{\rho_j-\rho_0}{\rho_0}, \text{ for } j=1,\cdots,n_s; \quad \text{and } R_c=\sum_{j=1}^{n_s}R_jc_j. \tag{2.2}$$

The source term ϕ_η represents the amount of ocean water entrained and mixed by turbulence to the plume.

The sediment flux at the bed of the jth specie is determined from the rates of deposition (F_d^j) and erosion (F_e^j),

$$\phi_b^j=F_e^j-F_d^j, \quad \phi_b=\sum_{j=1}^{n_s}\phi_b^j. \tag{2.3}$$

We denote $\xi=1/(1-\gamma)$, being γ the porosity of the sediment layer. Finally, τ represents the friction term.

There are some discrepancies in the mathematical expression of the source terms ϕ_η and ϕ_b. In particular the expressions proposed in [18,24] and [16] are among the most extended. According to these authors, the amount of ocean water ϕ_η entrained and mixed by turbulence to the plume, may be described as $E_w u$, where the water entrainment coefficient E_w, is determined for the empirical law:

$$E_w=\frac{0.00153}{0.0204+\mathcal{R}i}, \tag{2.4}$$

where the Richardson number, $\mathcal{R}i$ is defined as

$$\mathcal{R}i=\frac{R_c g h}{u^2}. \tag{2.5}$$

The rate of deposition is described as the product of the settling velocity of sediment, v_{s_j}, and the fractional concentration of suspension near by the bed, c_{b_j}. For multiple grain sizes, the sum of this product for each size population is used as the net rate of deposition

$$F_d^j = v_{s_j} c_{b_j}. \tag{2.6}$$

Different expressions for the near bed concentration can again be found in the literature. While in [13] and [2], c_{b_j} is considered to be a half of the layer-averaged concentration c_b, in [16] and [6] the following law is proposed

$$\frac{c_{b_j}}{c_j} = 0.4\left(\frac{D_j}{D_{sg}}\right)^{1.64} + 1.64, \tag{2.7}$$

where D_j is the characteristic grain size and D_{sg} denotes the geometric mean size of the suspended sediment mixture.

The rate of sediment entrainment from the bed is described as

$$F_e^j = v_{s_j} p_j E_{s_j}, \tag{2.8}$$

where the sediment entrainment coefficient, E_{s_j}, is given by the expression developed by Garcia and Parker [12],

$$E_{s_j} = \frac{1.3\cdot 10^{-7} Z_j^5}{1 + 4.3\cdot 10^{-7} Z_j^5}, \tag{2.9}$$

where

$$Z_j = \alpha_1 \frac{\sqrt{c_D}|u|}{v_{s_j}} \mathcal{R}_{p_j}^{\alpha_2}, \tag{2.10}$$

and

$$\mathcal{R}_{p_j} = \frac{\sqrt{R_j g D_j} D_j}{\nu} \tag{2.11}$$

is the particle Reynolds number, with ν the kinematic viscosity. The parameters (α_1,α_2) take the values $(1,0.6)$ for $\mathcal{R}_{p_j} > 2.36$ and $(0.586,1.23)$ for $\mathcal{R}_{p_j} \leq 2.36$. We remark again that this is not the only expression used in models describing the physics of the problem. Some variants can be found in [6, 17, 18].

In (2.8), p_j represents the volume fraction of the jth sediment in the bed. It could be described as a function of time as it is the case in [6].

The friction term τ is described as a function of the velocity,

$$\tau = -(1+\alpha) c_D |u| u, \tag{2.12}$$

where c_D is the bed drag coefficient which ranges from 0.002 to 0.05 depending on the flow type and α is the ratio of the drag force at the upper flow surface to that at the bed.

Finally, the fall velocity v_{s_j} may be calculated by using the empirical relationship introduced by Dietrich [11].

Let us show that some relevant features are missing in system (2.1). First, let us denote by c_0 the freshwater concentration in the plume and by c the summation of all of the sediment fractions. The relation $c_0=1-c$ is satisfied and from (2.1) one gets

$$\partial_t(c_0h)+\partial_x(c_0hu)=\phi_\eta-\phi_b. \tag{2.13}$$

This means that erosion and deposition effects *modify* the freshwater mass while it is clear that in absence of the water entrainment, $\phi_\eta=0$, freshwater mass should be preserved.

Another point is that deposition/erosion and water entrainment are not taken into account for the momentum equation. We will see in Section 3 that source terms related to the deposition/erosion and the water entrainment effects appear naturally in the momentum equation.

Notice also that the density of the ambient fluid ρ_w does not appear explicitly in the equations, so that the model is only useful when $\rho_w\approx\rho_0$.

Finally, the sediment transport of bed-load particles due to the velocity of the current is not taken into account. In the next section, after deriving the PDE system by depth averaging the Navier-Stokes equations by using some simplifying assumptions, we obtain the following expression for the system:

$$\begin{cases} \partial_t h+\partial_x(hu)=E_w u+\displaystyle\sum_{j=1}^{n_s} v_{s_j}(p_jE_{s_j}-c_{b_j}), \\ \partial_t(hu)+\partial_x\left(hu^2+g(R_0+R_c)\dfrac{h^2}{2}\right)=g(R_0+R_c)h\partial_x H \\ \qquad +E_w u^2+\dfrac{u}{2}\displaystyle\sum_{j=1}^{n_s} v_{s_j}(p_jE_{s_j}-c_{b_j})-(1+\alpha)c_D|u|u, \\ \partial_t(hc_j)+\partial_x(huc_j)=v_{s_j}(p_jE_{s_j}-c_{b_j}), \\ \partial_t H-\xi\partial_x q_b=\xi\displaystyle\sum_{j=1}^{n_s} v_{s_j}(p_jE_{s_j}-c_{b_j}). \end{cases} \tag{2.14}$$

Here,

$$R_0=\frac{\rho_0-\rho_w}{\rho_0}. \tag{2.15}$$

Sediment transport of bed-load particles due to the velocity of the current is represented by ξq_b where $\xi=1/(1-\gamma)$, being γ the porosity of the sediment layer, and q_b represents the solid transport flux, that depends on the fluid velocity u, $q_b=q_b(h,hu)$.

Several formulae for solid transport flux have been proposed, see [14,19,21], etc. Here, we shall consider the simplest one, which is the Grass model. According to it, the solid transport fluid equation is

$$q_b=A_g u|u|^{m_g-1},\quad 1\le m_g\le 4, \tag{2.16}$$

where A_g is a constant that represents the effects due to grain size and kinematic viscosity and is usually determined by experimental data. Usually, the constant m_g is set to $m_g=3$.

Even if some other expression of the solid transport flux is considered, most of what follows remains valid. The election of Grass model will only play an essential role in Lemma 4.2, where the explicit expression of the corresponding eigenvalues can be given, as well as in the explicit definition of a Roe matrix in Section 5.

Remark 2.1. We are mainly interested in the simulation of a river with a mixture of sediments that plunges into the ocean. In this case, ρ_w (saltwater density) is slightly greater than ρ_0 (freshwater density) and $R_0<0$. The case where the ambient fluid is air can also be considered: in that case $\rho_w\approx 0$ and $R_0\approx 1$.

Let us see that system (2.14) takes into account the missing effects:

- From (2.14) one gets
$$\partial_t(c_0h)+\partial_x(c_0hu)=\phi_\eta, \tag{2.17}$$
where $c_0=1-c$ is the freshwater concentration. There, if there is no ocean water entrainment, the total freshwater mass is preserved.
- The pressure term $gR_0h^2/2$ in the second equation allows to consider a turbid current that plunges into the ocean ($R_0\approx 0$) as well as currents flowing in the air ($R_0\approx 1$).
- The effects of deposition/erosion and water entrainment on the momentum equation have been taken into account.
- Solid transport of particles at the bottom has been included by means of a solid transport flux q_b.

3 Derivation of the layer-averaged equations

3.1 Governing equations for a dilute suspension

We consider the situation described in Section 1 and, in particular, in Fig. 1. In order to simulate only the turbidity current, the rigid lid hypothesis for the ambient fluid is assumed. The width of the plume is assumed to be small compared to the characteristic horizontal lengths, so that the shallow water hypothesis is finally justified.

The equations of motion for a suspension are considered. The suspension is assumed to be sufficiently dilute to justify the use of the Boussinesq approximation, and to consider that the value of the kinematic viscosity ν is equals to the corresponding to clear water. The equation of momentum conservation is

$$\frac{\partial\vec{u}}{\partial t}+\mathrm{div}(\vec{u}\otimes\vec{u})=-\frac{1}{\rho_0}\nabla p+\frac{1}{\rho_0}\nabla\cdot\mathcal{T}+(1+R_c)\vec{g}, \tag{3.1}$$

where $\vec{u}(\vec{x},t)$ represents the instantaneous velocity of the mixture, $p(\vec{x},t)$ denotes the instantaneous pressure, $\vec{g}=(0,0,-g)$ is the gravity, and

$$\mathcal{T}=\mu(\nabla\vec{u}+(\nabla\vec{u})^t) \tag{3.2}$$

is the stress tensor. We denote

$$c=\sum_{j=1}^{n_s}c_j,\quad R_0=1-\rho_w/\rho_0,\quad R_c=\sum_{j=1}^{n_s}R_jc_j,$$

where $R_j=\rho_j/\rho_0-1$ and $c_j(x,t)$, for $j=1,\cdots,n_s$ denotes the instantaneous volumetric concentration of the jth suspended sediment.

The fluid is assumed to be incompressible and the continuity equation is also considered:

$$\mathrm{div}\vec{u}=0, \tag{3.3}$$

$$\partial_t\rho+\mathrm{div}(\rho\vec{u})=0, \tag{3.4}$$

where ρ is the density of the turbidity current.

Following the notation of Section 2, we may rewrite the density of the current as

$$\rho=\sum_{j=0}^{n_s}(\rho_jc_j)=\rho_0\big(1+\sum_{j=1}^{n_s}R_jc_j\big), \tag{3.5}$$

where $c_0(\vec{x},t)$ denotes the portion of water in the turbidity current.

Now, as $\sum_{j=0}^{n_s}c_j=1$, from Eqs. (3.3) and (3.4) we get

$$\begin{aligned}0&=\partial_t\left(c_0\rho_0+\sum_{j=1}^{n_s}\rho_jc_j\right)+\mathrm{div}\left(\left(c_0\rho_0+\sum_{j=1}^{n_s}c_j\rho_j\right)\vec{u}\right)\\&=\partial_t\left(\sum_{j=1}^{n_s}c_j(\rho_j-\rho_0)\right)+\mathrm{div}\left(\sum_{j=1}^{n_s}c_j(\rho_j-\rho_0)\vec{u}\right).\end{aligned} \tag{3.6}$$

In order to satisfy (3.6), we shall assume that the volume fraction of each sediment specie satisfies the equation

$$\frac{\partial c_j}{\partial t}+\mathrm{div}(c_j\vec{u})=0,\quad \text{for } j=1,\cdots,n_s. \tag{3.7}$$

As a consequence, this relation is also satisfied by the volume fraction of freshwater and the equations of mass conservation are thus

$$\frac{\partial c_j}{\partial t}+\mathrm{div}(c_j\vec{u})=0,\quad \text{for } j=0,1,\cdots,n_s. \tag{3.8}$$

3.2 Vertically integrated equations

Henceforth $\vec{x}=(x,y,z)$ and $\vec{u}=(u,v,w)$. For simplicity, variations in the horizontal y direction are neglected and we suppose $v=0$.

As the current is considered to be two-dimensional, the region occupied by the flow is

$$\left\{(t,x,z)\in\mathbb{R}^+\times\mathbb{R}^2 / b(x,t)<z<b(x,t)+h(x,t)\right\}, \tag{3.9}$$

where $b(x,t)$ is the bottom elevation from a defined reference level and $h(x,t)$ is the length of the turbidity layer.

Perturbations of the free surface due to the turbidity current are neglected, so that the water surface is considered to be constant and equal to $z=H_0$. It will be useful to define the bottom depth from the surface

$$H(x,t)=H_0-b(x,t), \tag{3.10}$$

and the interface between the turbidity current and the ambient water

$$\eta(x,t)=b(x,t)+h(x,t). \tag{3.11}$$

Some kinematic conditions should be imposed at the bottom and at the interface. The turbidity current lies between an upper non-material interface,

$$F^s=z-\eta(x,t)=0,$$

and a basal interface,

$$F^b=b(x,t)-z=0.$$

These curves are defined so that their unit normals $n^s=\nabla F^s/|\nabla F^s|$ and $n^b=\nabla F^b/|\nabla F^b|$ point outwards from the turbidity current. Assuming that these interfaces have velocities $\vec{v}^s$ and $\vec{v}^b$, the kinematic boundary conditions are

$$F^s(x,z,t)=0: \quad \partial_t F^s+\vec{v}^s\cdot\nabla F^s=0, \tag{3.12}$$

$$F^b(x,z,t)=0: \quad \partial_t F^b+\vec{v}^b\cdot\nabla F^b=0. \tag{3.13}$$

The upper and basal interfaces are modified by entrainment of water from the above and deposition/erosion of sediment at the bottom. Let the normal entrainment rate, d^s, be the equivalent volume of ambient water entrained to the turbid current at the upper interface per unit area per unit time. Then the velocity of the interface is

$$\vec{v}^s=\vec{u}^s+d^s\vec{n}^s.$$

Similarly, if the normal deposition/erosion rate, d^b, is the equivalent volume of granular material deposited/eroded at the bottom per unit area per unit time, the velocity of the basal interface is

$$\vec{v}^b=\vec{u}^b+d^b\vec{n}^b.$$

It follows that the kinematic conditions (3.12)-(3.13) are

$$z=\eta(x,t): \quad \partial_t\eta+u^s\partial_x\eta-w^s=(1+(\partial_x\eta)^2)^{1/2}d^s, \tag{3.14}$$

$$z=b(x,t): \quad \partial_t b+u^b\partial_x b-w^b=-(1+(\partial_x b)^2)^{1/2}d^b. \tag{3.15}$$

Thus, we shall consider the kinematic equations

$$\partial_t\eta+u|_{z=\eta}\partial_x\eta-w|_{z=\eta}=\widetilde{\phi}_\eta, \tag{3.16}$$

$$\partial_t b+u|_{z=b}\partial_x b-w|_{z=b}=-\widetilde{\phi}_b, \tag{3.17}$$

where

$$\vec{u}=(u,w), \quad \widetilde{\phi}_\eta=(1+(\partial_x\eta)^2)^{1/2}d^s, \quad \widetilde{\phi}_b=(1+(\partial_x b)^2)^{1/2}d^b.$$

Under these hypothesis, mass conservation equations yield

$$\partial_t\int_b^\eta c_j dz+\partial_x\int_b^\eta c_j u dz=c_j|_{z=\eta}\widetilde{\phi}_\eta+c_j|_{z=b}\widetilde{\phi}_b, \text{ for } j=0,1,\cdots,n_s. \tag{3.18}$$

We shall only retain the vertical components of the stress tensor and assume that the other terms may be neglected. Let us denote by

$$\widetilde{\tau}=\frac{\mu}{\rho_0}\left(\frac{\partial u}{\partial z}+\frac{\partial w}{\partial x}\right) \tag{3.19}$$

the $(1,2)$ component of the stress tensor $\mathcal{T}$. Let us also suppose that the pressure p reduces to hydrostatic effects,

$$p(x,z,t)=\int_z^\eta\sum_{j=0}^{n_s}(\rho_j c_j)g dz'+g\rho_w(H_0-h-b). \tag{3.20}$$

By integrating the momentum equation, we obtain:

$$\begin{aligned}&\partial_t\int_b^\eta u dz+\partial_x\int_b^\eta u^2 dz+\frac{g}{\rho_0}\int_b^\eta\partial_x p dz-g\frac{\rho_w}{\rho_0}h\partial_x\eta\\&=\widetilde{\tau}|_{z=\eta}-\widetilde{\tau}|_{z=b}+u|_{z=\eta}\widetilde{\phi}_\eta+u|_{z=b}\widetilde{\phi}_b.\end{aligned} \tag{3.21}$$

Definition 3.1. *For any function $f(x,z,t)$ we define the mean of the function as*

$$\overline{f}=\frac{1}{h}\int_b^\eta f dz. \tag{3.22}$$

The fluctuating part of f relative to the mean is defined by

$$\widehat{f}=f-\overline{f}. \tag{3.23}$$

Using this notation, it is clear now that, given two functions f_1, f_2, one has

$$h\overline{f_1}\,\overline{f_2}+\int_b^\eta \widehat{f_1}\widehat{f_2}dz=\int_b^\eta f_1 f_2 dz. \tag{3.24}$$

Thus, Eq. (3.18) writes as follows:

$$\partial_t(h\overline{c_j})+\partial_x(h\overline{c_j}\,\overline{u})+\partial_x\left(\int_b^\eta \widehat{c_j}\widehat{u_j}dz\right)=c_j|_{z=\eta}\widetilde{\phi}_\eta+c_j|_{z=b}\widetilde{\phi}_b, \text{ for } j=0,1,\cdots,n_s. \tag{3.25}$$

From Eq. (3.20) we get

$$p(x,z,t)=g\sum_{j=0}^{n_s}(\rho_j\overline{c_j}(\eta-z))+g\rho_w(H_0-h-b)+g\int_z^\eta\sum_{j=0}^{n_s}(\rho_j\widehat{c_j})dz', \tag{3.26}$$

and

$$\begin{aligned}
&\int_b^\eta\frac{1}{\rho_0}\partial_x p dz-g\int_b^\eta\partial_x\left\{\int_z^\eta\sum_{j=0}^{n_s}(\rho_j\widehat{c_j})dz'\right\}dz\\
&=\frac{g}{\rho_0}\int_b^\eta\partial_x\left(\sum_{j=0}^{n_s}(\rho_j\overline{c_j})(\eta-z)\right)dz-g\frac{\rho_w}{\rho_0}h\partial_x(h+b)\\
&=\frac{g}{\rho_0}\partial_x\left(\int_b^\eta\sum_{j=0}^{n_s}(\rho_j\overline{c_j}(\eta-z))dz\right)+\frac{g}{\rho_0}\sum_{j=0}^{n_s}\rho_j\overline{c_j}h\partial_x b-g\frac{\rho_w}{\rho_0}h\partial_x(h+b)\\
&=g\partial_x\left(R_0+\sum_{j=1}^{n_s}R_j\overline{c_j}\frac{h^2}{2}\right)+g\left(R_0+\sum_{j=1}^{n_s}R_j\overline{c_j}\right)h\partial_x b.
\end{aligned}\tag{3.27}$$

Consequently, (3.21) can be written as follows:

$$\begin{aligned}
&\partial_t(h\overline{u})+\partial_x\left(h\overline{u}^2+g\left(R_0+\sum_{j=1}^{n_s}R_j\overline{c_j}\right)\frac{h^2}{2}\right)+g\left(R_0+\sum_{j=1}^{n_s}R_j\overline{c_j}\right)h\partial_x b\\
&\quad+\int_b^\eta\widehat{u}^2dz+g\int_b^\eta\partial_x\int_z^\eta\sum_{j=0}^{n_s}(\rho_j\widehat{c_j})dz'dz\\
&=\widetilde{\tau}|_{z=\eta}-\widetilde{\tau}|_{z=b}+u|_{z=\eta}\widetilde{\phi}_\eta+u|_{z=b}\widetilde{\phi}_b.
\end{aligned}\tag{3.28}$$

3.3 Similarity assumptions

In this point, it is necessary to make some assumptions in order to write the integrated equations in terms of the mean variables. We will assume that the fluctuating part of the variables c_j, $\widehat{c_j}$, are negligible. The term $\int_b^\eta\widehat{u}^2dz$ corresponds to the kinematic Reynolds

stress. We shall assume that this term together with the tensor stress may be expressed in terms of $\overline{u}$ so that we write

$$\widetilde{\tau}|_{z=\eta}-\widetilde{\tau}|_{z=b}-\int_b^\eta \widehat{u}^2dz=\tau(\overline{u}). \tag{3.29}$$

Let us finally consider the approximations

$$\phi_\eta^j\simeq c_j|_{z=\eta}\widetilde{\phi}_\eta,\quad \phi_b^j\simeq c_j|_{z=b}\widetilde{\phi}_b,\quad j=0,1,\cdots,n_s, \tag{3.30}$$

and

$$\phi_\eta=\sum_{j=0}^{n_s}\phi_\eta^j\simeq\widetilde{\phi}_\eta,\quad \phi_b=\sum_{j=0}^{n_s}\phi_b^j\simeq\widetilde{\phi}_b. \tag{3.31}$$

In particular, as there is no water entrainment at the bottom, we shall assume $\phi_b^0=0$, and ϕ_b^j for $j=1,\cdots,n_s$ will be given by the empirical relations described in Section 2. In the same way, there is no sediment transfer at the interface $z=\eta$ and we shall suppose $\phi_\eta^j=0$, for $j=1,\cdots,n_s$ and $\phi_\eta^0\equiv\phi_\eta$ described in Section 2.

It is usual to express the velocity at the surface and bottom $u|_{z=\eta}$ and $u|_{z=b}$ in terms of the mean velocity $\overline{u}$, see for example [3,24] and [15]. Actually, the velocity profile with depth is rather blunt and shear is confined to a very thin layer. Entropy considerations presented in [3] leads us to assume $u|_{z=\eta}=\overline{u}$ and $u|_{z=b}=\frac{1}{2}\overline{u}$.

Thus, using the fact that $c_0=1-c$ and $\partial_x b=-\partial_x H$ we arrive to the final model

$$\begin{cases}\partial_t h+\partial_x(h\overline{u})=\phi_\eta+\phi_b,\\ \partial_t(h\overline{c})+\partial_x(h\overline{u}\,\overline{c})=\phi_b,\\ \partial_t(h\overline{u})+\partial_x\left(h\overline{u}^2+g(R_0+R_c)\frac{h^2}{2}\right)=g(R_0+R_c)h\partial_x H+\overline{u}\phi_\eta+\frac{\overline{u}}{2}\phi_b+\tau.\end{cases} \tag{3.32}$$

The second equation will be replaced by one equation for each sediment specie,

$$\partial_t(h\overline{c_j})+\partial_x(h\overline{u}\,\overline{c_j})=\phi_b^j,\text{ for } j=1,\cdots,n_s, \tag{3.33}$$

where $\sum_{j=1}^{n_s}\phi_b^j=\phi_b$.

3.4 Evolution of the topography

Sediment and erosion of the bottom as well as sediment transport due to the velocity of the current are considered here. The bed-sediment conservation equation has the form

$$\partial_t b+\xi\partial_x q_b=-\xi\phi_b, \tag{3.34}$$

where $q_b=q_b(h,h\overline{u})$ denotes the solid transport flow and $\xi=\frac{1}{1-\gamma}$, where γ is the porosity of the bed.

4 Reformulation and properties of the model

The system may be rewritten in the form:

$$\partial_t W+\partial_x \widetilde{F}(W)=B(W)\partial_x W+S(W), \tag{4.1}$$

where

$$W=(h,hu,hc_1,\cdots,hc_{n_s},H)^t, \quad B(W)=g(R_0+R_c)he_{2,n_s+3},$$
$$\widetilde{F}(W)=(hu,hu^2+g/2(R_0+R_c)h^2,hc_1u,\cdots,hc_{n_s}u,-\xi q_b)^t,$$

and

$$S(W)=\begin{pmatrix} E_w u+\sum_{j=1}^{n_s} v_{s_j}(p_jE_{s_j}-c_{b_j}) \\ E_w u^2+\frac{u}{2}\sum_{j=1}^{n_s} v_{s_j}(p_jE_{s_j}-c_{b_j})-(1+\alpha)c_D|u|u \\ v_{s_1}(p_1E_{s_1}-c_{b_1}) \\ \cdots \\ v_{s_{n_s}}(p_{n_s}E_{s_{n_s}}-c_{b_{n_s}}) \\ \xi\sum_{j=1}^{n_s} v_{s_j}(p_jE_{s_j}-c_{b_j}) \end{pmatrix}. \tag{4.2}$$

Here $e_{r,s}=(\delta_{ir}\delta_{js})_{i=1,j=1}^{n_s+3,n_s+3}$ is the canonical basis of square matrices of order n_s+3.

We will also use the notation

$$U=(h,hu,hc_1,\cdots,hc_{n_s})^t, \quad F(U)=(hu,hu^2+g/2(R_0+R_c)h^2,hc_1u,\cdots,hc_{n_s}u)^t.$$

The problem may also be written in the more general form

$$\partial_t W+\mathcal{A}(W)\partial_x W=S(W), \tag{4.3}$$

where $\mathcal{A}=\nabla\widetilde{F}(W)-B(W)$. More explicitly,

$$\mathcal{A}(W)=\begin{pmatrix} 0 & 1 & 0 & 0 & \cdots & 0 & 0 \\ gh(R_0+\frac{1}{2}R_c)-u^2 & 2u & \frac{g}{2}R_1h & \frac{g}{2}R_2h & \cdots & \frac{g}{2}R_{n_s}h & -g(R_0+R_c)h \\ -c_1u & c_1 & u & 0 & \cdots & 0 & 0 \\ -c_2u & c_2 & 0 & u & \cdots & 0 & 0 \\ \cdots & \cdots & \cdots & \cdots & \cdots & \cdots & \cdots \\ -c_{n_s}u & c_{n_s} & 0 & 0 & \cdots & u & \cdots \\ -\xi\frac{\partial q_b}{\partial h} & -\xi\frac{\partial q_b}{\partial(hu)} & 0 & 0 & \cdots & 0 & 0 \end{pmatrix}. \tag{4.4}$$

Theorem 4.1. *Suppose $R_0h+R_ch>0$ and ∇q_b sufficiently small. Then, the system (4.3) is hyperbolic. Moreover, even though it is not strictly hyperbolic for $n_s>1$, one can always find a complete set of eigenvector for $\mathcal{A}$ in $\mathbb{R}^{n_s+3}$.*

Proof. This is a consequence of the following lemma. □

Lemma 4.1. *Consider the matrix*

$$\mathcal{A}=\begin{pmatrix} 0 & 1 & 0 & 0 & \cdots & 0 & 0 \\ g(R_0h+\frac{1}{2}\gamma)-u^2 & 2u & \frac{g}{2}R_1h & \frac{g}{2}R_2h & \cdots & \frac{g}{2}R_{n_s}h & -g(R_0h+\gamma) \\ -c_1u & c_1 & u & 0 & \cdots & 0 & 0 \\ -c_2u & c_2 & 0 & u & \cdots & 0 & 0 \\ \cdots & \cdots & \cdots & \cdots & \cdots & \cdots & \cdots \\ -c_{n_s} & c_{n_s} & 0 & 0 & \cdots & u & 0 \\ \alpha & \beta & 0 & 0 & \cdots & 0 & 0 \end{pmatrix} \tag{4.5}$$

and suppose $R_0h+\frac{\gamma}{2}+\frac{1}{2}R_ch>0$. *There exists* $\varepsilon>0$ *such that if* $\alpha^2+\beta^2<\varepsilon$, *then the matrix* $\mathcal{A}$ *has* n_s+3 *real eigenvalues, being* $\lambda=u$ *an eigenvalue of multiplicity at least* n_s. *Moreover, if there are four different eigenvalues, a basis of eigenvectors can be found.*

Proof. Some easy calculations show that the characteristic polynomial of $\mathcal{A}$ is

$$p(\lambda)=-(u-\lambda)^{n_s}q(\lambda), \tag{4.6}$$

where

$$q(\lambda)=\lambda^3+a_2\lambda^2+a_1\lambda+a_0, \tag{4.7a}$$
$$a_2=-2u, \tag{4.7b}$$
$$a_1=u^2-g(R_0h+\frac{\gamma}{2}+\frac{1}{2}R_ch)+g(R_0h+\gamma)\beta, \tag{4.7c}$$
$$a_0=g(R_0h+\gamma)\alpha. \tag{4.7d}$$

Thus, u is an eigenvalue of multiplicity at least n_s.

In the particular case $\alpha=\beta=0$, the eigenvalues are

$$\lambda_1=u-\sqrt{g(R_0h+\frac{\gamma}{2}+\frac{1}{2}R_ch)}, \tag{4.8a}$$
$$\lambda_2=u+\sqrt{g(R_0h+\frac{\gamma}{2}+\frac{1}{2}R_ch)}, \tag{4.8b}$$
$$\lambda_{2+j}=u, j=1,\cdots,n_s, \tag{4.8c}$$
$$\lambda_{n_s+3}=0. \tag{4.8d}$$

By continuity, the matrix has n_s+3 real eigenvalues for $\alpha^2+\beta^2$ sufficiently small.

Now, denote by $\lambda_1,\lambda_2,\lambda_3$ the roots of the polynomial $q(\lambda)$ and assume they are different real numbers not equal to u. If $r=(x,y,w_1,\cdots,w_n,z)^t$ is an eigenvector of $\mathcal{A}$ corre-

sponding to the eigenvalue λ, then

$$\begin{cases} y=\lambda x, \\ (\lambda^2+u^2-g(R_0h+\frac{\gamma}{2})-2u\lambda)x=\sum_{j=1}^{n_s}\frac{g}{2}R_jw_jh-g(R_0h+\gamma)z, \\ c_j(\lambda-u)x=(\lambda-u)w_j, \text{ for } j=1,\cdots,n_s, \\ (\alpha+\beta\lambda)x=\lambda z. \end{cases} \tag{4.9}$$

We shall consider some different cases:

A) Case $\lambda\in\{\lambda_1,\lambda_2,\lambda_3\}$

A.1) Case $\lambda\neq 0$. As λ is a root of the polynomial q, one has

$$(\lambda-u)^2-g(R_0h+\frac{\gamma}{2}+\frac{1}{2}R_ch)=-g(R_0h+\gamma)(\alpha+\beta\lambda)\lambda^{-1}. \tag{4.10}$$

Thus, the system (4.9) reduces to

$$\begin{cases} y=\lambda x, \\ (R_0h+\gamma)(\alpha+\beta\lambda)\lambda^{-1}x=(R_0h+\gamma)z, \\ c_jx=w_j, \text{ for } j=1,\cdots,n_s, \\ (\alpha+\beta\lambda)x=\lambda z, \end{cases} \tag{4.11}$$

and one can easily check that the following vector is an eigenvector:

$$r=(\lambda,\lambda^2,\lambda c_1,\cdots,\lambda c_n,\alpha+\beta\lambda)^t. \tag{4.12}$$

A.2) Case $\lambda=0$. In this case, we have $a_0=g(R_0h+\gamma)\alpha=0$ and system (4.9) reduces to

$$\begin{cases} y=0, \\ (u^2-g(R_0h+\frac{\gamma}{2}+\frac{1}{2}R_ch))x=-g(R_0h+\gamma)z, \\ c_jx=w_j, \text{ for } j=1,\cdots,n_s, \\ \alpha x=0. \end{cases} \tag{4.13}$$

We set

$$r=\begin{cases} (0,0,\cdots,0,1)^t, & \text{if } \alpha\neq 0, \\ (-g(R_0h+\gamma),0,-g(R_0h+\gamma)c_1,\cdots, & \\ \quad -g(R_0h+\gamma)c_n,u^2-g(R_0h+\gamma/2+R_ch/2))^t, & \\ & \text{if } \alpha=0 \text{ and } u^2-g(R_0h+\gamma/2+R_ch/2)\neq 0, \\ (1,0,c_1,\cdots,c_n,0), & \text{if } \alpha=0 \text{ and } u^2-g(R_0h+\gamma/2+R_ch/2)=0, \end{cases} \tag{4.14}$$

which defines an eigenvector for $\lambda=0$.

B) Case $\lambda=u$

Any eigenvector associated to u should verify

$$\begin{cases} y=ux, \\ -(R_0h+\dfrac{\gamma}{2})x=\dfrac{1}{2}\displaystyle\sum_{j=1}^{n_s}R_jw_jh-(R_0h+\gamma)z, \\ (\alpha+\beta u)x=uz. \end{cases} \tag{4.15}$$

Thus, define for $j=1,\cdots,n_s$

$$r_j=\frac{1}{2}R_jh(u,u^2,0,\cdots,0,\alpha+\beta u)+\Big((\alpha+\beta u)(R_0h+\gamma)-u(R_0h+\frac{\gamma}{2})\Big)e_{j+2}, \tag{4.16}$$

where $e_i, i=1,\cdots,n_s+3$ represents the ith element of the canonical basis in $\mathbb{R}^{n_s+3}$. They form a set of n_s independent eigenvectors corresponding to u as long as

$$(\alpha+\beta u)(R_0h+\gamma)-u(R_0h+\frac{\gamma}{2})\neq 0.$$

Now, if $(\alpha+\beta u)(R_0h+\gamma)=u(R_0h+\frac{\gamma}{2})$, then $u\neq 0$ (otherwise, we would have $a_0=0$ and $u=0$ of multiplicity at least n_s+1 so there are only 3 different eigenvalues). Thus, system (4.9) writes

$$\begin{cases} y=ux, \\ \displaystyle\sum_{j=1}^{n_s}R_jw_jh=0, \\ (\alpha+\beta u)x=uz, \end{cases} \tag{4.17}$$

and we may define a set of n_s independent eigenvectors by

$$r_1=(u,u^2,0,\cdots,0,\alpha+\beta u), \tag{4.18a}$$
$$r_j=r_1-R_je_{j+1}+R_{j-1}e_{j+2}, \text{ for } j=2,\cdots,n_s. \tag{4.18b}$$

This completes the proof of this lemma. □

Lemma 4.2. *Suppose that the solid transport flux q_b is given by the Grass model* (2.16)*. Then if $R_0+R_c>0$ all the eigenvalues of* (4.4) *are real.*

Proof. In this particular case, the coefficients of the polynomial (4.7a) are

$$a_2=-2u, \tag{4.19a}$$
$$a_1=u^2-g_ch(1+d), \tag{4.19b}$$
$$a_0=g_chud, \tag{4.19c}$$

where

$$g_c=g(R_0+R_c), \quad d=\xi\frac{\partial q_b}{\partial(hu)}=\xi\frac{1}{h}A_gm_g|u|^{m_g-1}.$$

According to the Cardano-Vieta relations, the roots of $q(\lambda)$ are real if $Q^3+R^2<0$, where

$$Q=\frac{3a_1-a_2^2}{9},\quad R=\frac{9a_1a_2-27a_0-2a_2^3}{54}. \tag{4.20}$$

In that case, the eigenvalues are given by

$$\lambda_i=2\sqrt{-Q}\cos\left(\frac{\theta+2^{i-1}\pi}{3}\right)-\frac{a_2}{3},\quad i=1,2,3, \tag{4.21}$$

with

$$\theta=\arccos\left(\frac{R}{\sqrt{-Q^3}}\right). \tag{4.22}$$

Some simple calculations show that

$$Q=\frac{-1}{9}(u^2+3g_ch(d+1)), \tag{4.23a}$$

$$R=\frac{u}{54}(9g_ch(2-d)-2u^2), \tag{4.23b}$$

$$Q^3=-\frac{1}{3^6}(u^6+3^2u^4g_ch(d+1)+3^3u^2g_c^2h^2(d+1)^2+3^3g_c^3h^3(d+1)^3, \tag{4.23c}$$

$$R^2=\frac{u^2}{2^2\cdot3^6}(3^4g_c^2h^2(2-d)^2+2^2u^4-2^2\cdot3^2u^2g_ch(2-d)). \tag{4.23d}$$

Thus, $Q^3+R^2<0$ as long as

$$\begin{aligned}&3^4g_c^2h^2u^2(2-d)^2-3^2\cdot2^2u^4g_ch(2-d)\\&<3^2\cdot2^2u^4g_ch(d+1)+3^3\cdot2^2u^2h^2g_c^2(d+1)^2+3^3\cdot2^2g_c^3h^3(d+1)^3,\end{aligned} \tag{4.24}$$

which is equivalent to

$$8g_c^2h^2u^2<2^2g_chu^4+g_c^2h^2u^2d(14+d)+2^2g_c^3h^3(d+1)^3. \tag{4.25}$$

By hypothesis $g_c>0$. Thus, (4.25) is equivalent to

$$\begin{aligned}0&<-8g_ch^2u^2+2^2hu^4+g_ch^2u^2d(14+d)+2^2g_c^2h^3(d+1)^3\\&=4h(u^2-g_ch)^2+g_chd(14+d)+4g_c^2h^3(d^3+3d^2+3d)\end{aligned} \tag{4.26}$$

and the result follows. □

Let us now investigate the possibility of finding an entropy pair for the system. We show first the following general result:

Proposition 4.1. *Consider the system*

$$\partial_t h+\partial_x(hu)=\phi_\eta+\phi_b, \tag{4.27a}$$

$$\partial_t(hu)+\partial_x\left(hu^2+g(R_0+R_c)\frac{h^2}{2}\right)=g(R_0+R_c)h\partial_x H+u\phi_\eta+\frac{u}{2}\phi_b+\tau, \tag{4.27b}$$

$$\partial_t(hc_j)+\partial_x(huc_j)=\phi_b^j, \text{ for } j=1,\cdots,n_s, \tag{4.27c}$$

$$\partial_t H=\phi_b. \tag{4.27d}$$

Any smooth solution of (4.27) *satisfies the equation*

$$\begin{aligned}&\partial_t(\eta(W))+\partial_x(G(W))\\&=\left(\frac{u^2}{2}+g\left(R_0(h-H)+\frac{R_c h}{2}\right)\right)\phi_\eta-g\frac{R_c h}{2}\phi_b+g\left(\frac{h}{2}-H\right)\sum_{j=1}^{n_s}R_j\phi_b^j+u\tau,\end{aligned} \tag{4.28}$$

with

$$\eta(W)=h\frac{u^2}{2}+g(R_0+R_c)\frac{h^2}{2}-g(R_0+R_c)hH+gR_0\frac{H^2}{2}, \tag{4.29a}$$

$$G(W)=hu\left(\frac{u^2}{2}+g(R_0+gR_c)(h-H)\right). \tag{4.29b}$$

Proof. First, from Eqs. (4.27a) and (4.27b) we get:

$$\partial_t u+\partial_x\left(\frac{u^2}{2}\right)+\frac{1}{h}\partial_x\left(g(R_0+R_c)\frac{h^2}{2}\right)=g(R_0+R_c)\partial_x H-\frac{1}{2}\frac{u}{h}\phi_b+\frac{\tau}{h}. \tag{4.30}$$

Now, multiplying Eq. (4.27a) by $\frac{u^2}{2}+gR_0(h-H)$ and Eq. (4.30) by hu and adding the results we get

$$\begin{aligned}&\partial_t\left(h\frac{u^2}{2}+gR_0(\frac{h^2}{2}-Hh)\right)+\partial_x\left(hu\left(\frac{u^2}{2}+gR_0(h-H)\right)\right)+u\partial_x\left(gR_c\frac{h^2}{2}\right)\\&=ghuR_c\partial_x H-\frac{u^2}{2}\phi_b+\left(\frac{u^2}{2}+gR_0(h-H)\right)(\phi_\eta+\phi_b)-gR_0h\partial_t H+u\tau.\end{aligned} \tag{4.31}$$

The third term of the right hand side can be rewritten as follows:

$$\begin{aligned}&u\partial_x\left(gR_c\frac{h^2}{2}\right)=\partial_x\left(gR_c\frac{h^2}{2}u\right)-gR_c\frac{h}{2}\partial_x(hu)+gR_c\frac{h}{2}u\partial_x h\\&=\partial_x\left(gR_c\frac{h^2}{2}u\right)+gR_c\frac{h}{2}(\partial_t h-(\phi_\eta+\phi_b))+gR_c\frac{h}{2}u\partial_x h+g\frac{h}{2}\sum_{j=1}^{n_s}R_j(\partial_t(c_j h)+\partial_x(hc_j u)-\phi_b^j)\\&=\partial_t\left(gR_c\frac{h^2}{2}\right)+\partial_x\left(gR_c uh^2\right)-\frac{g}{2}R_c h(\phi_\eta+\phi_b)-\frac{g}{2}h\sum_{j=1}^{n_s}R_j\phi_b^j.\end{aligned} \tag{4.32}$$

Using this expression in (4.31) we get

$$\begin{aligned}&\partial_t\left(h\frac{u^2}{2}+g(R_0+R_c)\frac{h^2}{2}-gR_0Hh\right)+\partial_x\left(hu\left(\frac{u^2}{2}+g(R_0+R_c)h-gR_0H\right)\right)\\&=gR_chu\partial_xH-gR_0h\partial_tH+gR_0(h-H)(\phi_\eta+\phi_b)\\&\quad+\left(\frac{u^2}{2}+gR_c\frac{h}{2}\right)\phi_\eta+\frac{g}{2}R_ch\phi_b+\frac{g}{2}h\sum_{j=1}^{n_s}R_j\phi_b^j+u\tau.\end{aligned}\tag{4.33}$$

Now, we remark

$$\begin{aligned}&gR_chu\partial_xH-gR_0h\partial_tH+gR_0(h-H)(\phi_\eta+\phi_b)\\&=gR_chu\partial_xH+gR_0h(\phi_b-\partial_tH)-gR_0H(\phi_\eta+\phi_b)\\&\quad+gR_0h\phi_\eta+gH\sum_{j=1}^{n_s}R_j(\partial_t(hc_j)+\partial_x(hc_ju)-\phi_b^j)\\&=\partial_t(gR_chH)+\partial_x(gR_chuH)-gR_ch\partial_tH-gR_0H(\phi_\eta+\phi_b)+gR_0h\phi_\eta-gH\sum_{j=1}^{n_s}R_j\phi_b^j.\end{aligned}\tag{4.34}$$

Using this result in (4.33) we obtain (4.28). □

The above result shows that (η,G) is an entropy pair if some further assumptions are considered:

Corollary 4.1. *Consider the system* (4.27) *and suppose that the following assumptions are satisfied:*

$$\begin{aligned}&(i)\ \phi_\eta=0,\quad (ii)\ \phi_b\le 0,\\&(iii)\ u\tau\le 0,\quad (iv)\ R_j=\bar{R}\ \text{for}\ j=1,\cdots,n_s.\end{aligned}$$

Then, any smooth solution of (4.27) *satisfies the entropy inequality*

$$\partial_t(\bar{\eta}(W)+\frac{g}{2}\bar{R}H^2)+\partial_xG(W)\le 0,\tag{4.35}$$

where η and G are given by (4.29*a*) *and* (4.29*b*) *respectively.*

Proof. The following equality can be easily verified by using (iv).

$$-\frac{g}{2}hR_c\phi_b+\frac{g}{2}h\sum_{j=1}^{n_s}R_j\phi_b^j-gH\sum_{j=1}^{n_s}R_j\phi_b^j=\frac{g}{2}h\bar{R}(1-c)\phi_b-gH\bar{R}\phi_b.\tag{4.36}$$

Using this equality and 4.27d we may write (4.28) in the form

$$\begin{aligned}&\partial_t\left(\eta(W)+g\bar{R}\frac{H^2}{2}\right)+\partial_x(G(W))\\&=\left(\frac{u^2}{2}+g\left(R_0(h-H)+\frac{R_ch}{2}\right)\right)\phi_\eta+\frac{g}{2}h\bar{R}(1-c)\phi_b+u\tau,\end{aligned}\tag{4.37}$$

and the result follows. □

Concerning the hypothesis of Corollary 4.1, notice that (iii) is natural as τ represents a friction term and its sign is the opposite of u. On the other hand, as the source term ϕ_b is given by

$$\phi_b = \sum_{j=1}^{n_s} v_{s_j}(p_j E_{s_j} - c_{b_j}), \tag{4.38}$$

$\phi_b \leq 0$ as long as $c_{b_j} \geq p_j E_{s_j}$ i.e., if the deposition predominates over erosion. Given the definition of E_{s_j} in (2.9), this is the case in many physical situations.

Notice that $\eta(W)$ is the mechanical energy of the system. When $\phi_\eta \neq 0$, $\phi_b > 0$ or the sediments have different densities, the momentum equations of the ambient water and of the bottom should be included to be able to prove that the total mechanical energy cannot increase.

5 Numerical scheme

As usual, we consider a set of computing cells $I_i = [x_{i-1/2}, x_{i+1/2}], i \in \mathbb{Z}$. For the sake of simplicity, we assume that these cells have a constant size $\triangle x$ and that $x_{i+1/2} = i\triangle x$. $x_i = (i-1/2)\triangle x$ is the center of the cell I_i. Let $\triangle t$ be the time step and $t^n = n\triangle t$.

We denote by W_i^n the approximation of the cell averages of the exact solution

$$W_i^n \cong \frac{1}{\triangle x}\int_{x_{i-1/2}}^{x_{i+1/2}} W(x,t^n)dx. \tag{5.1}$$

Given the approximations (W_i^n) at time t_n, we compute the approximations at time t^{n+1} using a two-step algorithm.

First we solve

$$\begin{cases} \partial_t W + \partial_x \widetilde{F}(W) = B(W)\partial_x H, \\ W(x, t = t^n) = W_i^n \text{ for } x \in I_i. \end{cases} \tag{5.2}$$

Let $W_i^{n+1/2}$ be the approximations of the cell averages of the solution of this problem. We define

$$W_i^{n+1} = W_i^{n+1/2} + \triangle t S(W_i^n). \tag{5.3}$$

In order to solve (5.2), we introduce the theory described in [22, 23]. We briefly describe thereafter the application of the theory to the system considered here.

5.1 A Roe scheme for system (5.2)

System (5.2) may be written under the form

$$\frac{\partial W}{\partial t} + \mathcal{A}(W)\frac{\partial W}{\partial x} = 0, \quad x \in \mathbb{R},\ t > 0. \tag{5.4}$$

with $\mathcal{A}(W)$ defined by (4.4). This matrix has the following block structure

$$\mathcal{A}(W)=\left[\begin{array}{c|c}\mathcal{J}(U) & -b(U)\\ \hline -\xi\nabla q_b & 0\end{array}\right], \tag{5.5}$$

where $U=(h,hu,hc_1,\cdots,hc_{n_s})^t$, $\mathcal{J}(U)=\nabla_U F$, $F(U)=(hu,hu^2+g/2(R_0+R_c)h^2,hc_1u,\cdots,hc_{n_s}u)^t$ and $b(U)=(0,-g(R_0h+R_ch),0,\cdots,0)^t$.

Only the cases $q_b=0$ or q_b given by Grass model will be considered here.

Observe that system (5.4) contains a non-conservative product $\mathcal{A}(W)\cdot W_x$ which, in general, does not make sense within the framework of the theory of distributions. After the theory developed by Dal Masso, LeFloch, and Murat [10], a rigorous definition of weak solutions can be performed using a family of paths. We refer to [10, 22, 23] for further details.

In [25] a generalization of Roe methods to systems of the form (5.4) was introduced. These methods are based on the following general definition of a *Roe linearization*:

Definition 5.1. *Given a family of paths Ψ, a matrix function $\mathcal{A}_\Psi:\Omega\times\Omega\to\mathcal{M}_N(\mathbb{R})$ is called a Roe linearization if it satisfies:*

- *for any $W_L,W_R\in\Omega$, $\mathcal{A}_\Psi(W_L,W_R)$ has N real eigenvalues;*
- *$\mathcal{A}_\Psi(W,W)=\mathcal{A}(W)$, for all $W\in\Omega$;*
- *for any $W_L,W_R\in\Omega$:*

$$\mathcal{A}_\Psi(W_L,W_R)\cdot(W_R-W_L)=\int_0^1\mathcal{A}\big(\Psi(s;W_L,W_R)\big)\frac{\partial\Psi}{\partial s}(s;W_L,W_R)ds. \tag{5.6}$$

A family of paths is a Lipschitz continuous function $\Psi:[0,1]\times\Omega\times\Omega\to\Omega$ which must satisfy some regularity and compatibility conditions (see [10] for the details). In particular,

$$\Psi(0,W_l,W_r)=W_l,\quad \Psi(1,W_l,W_r)=W_r),\quad \Psi(s,W,W)=W.$$

Once a Roe linearization has been given, the corresponding Roe scheme can be written in the form

$$W_i^{n+1}=W_i^n-\frac{\Delta t}{\Delta x}\Big(\mathcal{A}^+_{i-1/2}\cdot(W_i^n-W_{i-1}^n)+\mathcal{A}^-_{i+1/2}\cdot(W_{i+1}^n-W_i^n)\Big), \tag{5.7}$$

where

$$\mathcal{L}^\pm_{i+1/2}=\left[\begin{array}{ccc}(\lambda_1^{i+1/2})^\pm & & 0\\ & \ddots & \\ 0 & & (\lambda_N^{i+1/2})^\pm\end{array}\right],\quad \mathcal{A}^\pm_{i+1/2}=\mathcal{K}_{i+1/2}\mathcal{L}^\pm_{i+1/2}\mathcal{K}^{-1}_{i+1/2}, \tag{5.8}$$

$\lambda_1^{i+1/2},\cdots,\lambda_N^{i+1/2}$ being the eigenvalues of $\mathcal{A}_{i+1/2}$ and $\mathcal{K}_{i+1/2}$ a matrix whose columns form a basis of associated eigenvectors.

We consider here the canonical choice of the family of paths

$$\Psi(s;W_L,W_R)=W_L+s(W_R-W_L). \tag{5.9}$$

The numerical scheme (5.7) is path-conservative in the sense of [22] for this family. In particular, this fact ensures that the numerical scheme is conservative in the usual sense for (4.27a), (4.27c), and (4.27d) if $\phi_\eta=\phi_b=\phi_b^j=0$, $j=1,\cdots,n_s$.

In order to build a Roe linearization based on the family of paths (5.9), it is natural to look for matrices with the same structure of $\mathcal{A}(W)$ (see [23])

$$\mathcal{A}_{i+1/2}=\left[\begin{array}{c|c} \mathcal{J}_{i+1/2} & -b_{i+1/2} \\ \hline -\xi q_{i+1/2} & 0 \end{array}\right]. \tag{5.10}$$

For Roe matrices with this structure, (5.6) can be rewritten as follows:

$$\mathcal{J}_{i+1/2}(U_{i+1}-U_i)-(H_{i+1}-H_i)b_{i+1/2}=F(U_{i+1})-F(U_i)-b_\Psi(W_i,W_{i+1}), \tag{5.11a}$$
$$q_{i+1/2}(U_{i+1}-U_i)=q_b(U_{i+1})-q_b(U_i), \tag{5.11b}$$

where

$$\begin{aligned} &b_\Psi(W_i,W_{i+1}) \\ &=\left[0,\int_0^1 g\left(R_0\Psi_1(s,W_i,W_{i+1})+\sum_{j=1}^{n_s}R_j\Psi_{j+2}(s,W_i,W_{i+1})\right)\frac{\partial\Psi_2}{\partial s}ds,0,\cdots,0\right]^t. \end{aligned} \tag{5.12}$$

In the particular case that q_b corresponds to Grass model, properties (5.11a)-(5.11b) are satisfied if we define:

$$\mathcal{J}_{i+1/2}=\begin{pmatrix} 0 & 1 & 0 & \cdots & 0 \\ g(R_0h_{i+1/2}+\frac{1}{2}\gamma_{i+1/2})-(u_{i+1/2})^2 & 2u_{i+1/2} & \frac{g}{2}R_1h_{i+1/2} & \cdots & \frac{g}{2}R_{n_s}h_{i+1/2} \\ -(c_1)_{i+1/2}u_{i+1/2} & (c_1)_{i+1/2} & u_{i+1/2} & \ddots & 0 \\ \cdots & \cdots & \cdots & \cdots & \cdots \\ -(c_{n_s})_{i+1/2} & (c_{n_s})_{i+1/2} & 0 & \cdots & u_{i+1/2} \end{pmatrix}, \tag{5.13a}$$

$$-\xi q_{i+1/2}=\begin{pmatrix} u_{i+1/2}d_{i+1/2} & -d_{i+1/2} & 0 & \cdots & 0 \end{pmatrix}, \tag{5.13b}$$

$$b_{i+1/2}=\begin{pmatrix} 0 \\ g(R_0h_{i+1/2}+\gamma_{i+1/2}) \\ 0 \\ \cdots \\ 0 \end{pmatrix}, \tag{5.13c}$$

where

$$h_{i+1/2}=\frac{h_i+h_{i+1}}{2},\quad u_{i+1/2}=\frac{\sqrt{h_i}u_i+\sqrt{h_{i+1}}u_{i+1}}{\sqrt{h_i}+\sqrt{h_{i+1}}},\tag{5.14a}$$

$$(c_j)_{i+1/2}=\frac{\sqrt{h_i}(c_j)_i+\sqrt{h_{i+1}}(c_j)_{i+1}}{\sqrt{h_i}+\sqrt{h_{i+1}}},\quad \gamma_{i+1/2}=\frac{\sum_{j=1}^{n_s}R_j((hc_j)_i+(hc_j)_{i+1})}{2},\tag{5.14b}$$

$$d_{i+1/2}=\frac{A_g\xi(\sqrt{h_i}+\sqrt{h_{i+1}})}{\sqrt{h_i}h_{i+1}+\sqrt{h_{i+1}}h_i}\sum_{k=0}^{m_g-1}(u_{i+1})^k(u_i)^{m_g-(k+1)}.\tag{5.14c}$$

The eigenstructure of matrices (5.10) is given by Lemma 4.1, and thus $\mathcal{A}_{i+1/2}$ is a Roe matrix.

Remark 5.1. If we neglect the solid transport flow ($q_b=0$), the system reduces to a system of conservation laws with a source term. Thus, following [23], we have

$$\mathcal{A}^{\pm}_{i+1/2}=\left[\begin{array}{c|c}\mathcal{J}^{\pm}_{i+1/2} & -\mathcal{J}^{\pm}_{i+1/2}\mathcal{J}^{-1}_{i+1/2}b_{i+1/2}\\ \hline 0 & 0\end{array}\right]\tag{5.15}$$

and the scheme (5.7) may be rewritten under the form

$$\begin{aligned}U_i^{n+1}=U_i^n-\frac{\triangle t}{\triangle x}\Big[&P^+_{i-1/2}(\mathcal{J}_{i-1/2}(U_i-U_{i-1})-b_{i-1/2}(H_i-H_{i-1}))\\&+P^-_{i+1/2}(\mathcal{J}_{i+1/2}(U_{i+1}-U_i)-b_{i+1/2}(H_{i+1}-H_i))\Big],\end{aligned}\tag{5.16}$$

where

$$P^{\pm}_{i+1/2}=\frac{1}{2}\Big(Id\pm|\mathcal{J}_{i+1/2}|\mathcal{J}^{-1}_{i+1/2}\Big).\tag{5.17}$$

5.2 The non-hyperbolic case

From Lemma 4.1, if

$$R_0h_{i+1/2}+\frac{1}{2}\gamma_{i+1/2}+\frac{1}{2}\sum_{j=1}^{n_s}(R_jc_j)_{i+1/2}h_{i+1/2}>0$$

and $d_{i+1/2}$ is sufficiently small, $\mathcal{A}_{i+1/2}$ has n_s+3 real eigenvalues that can be approached by

$$\lambda_1\simeq u_{i+1/2}-\sqrt{g(R_0h_{i+1/2}+\frac{\gamma_{i+1/2}}{2}+\frac{1}{2}(R_c)_{i+1/2}h_{i+1/2})},\tag{5.18a}$$

$$\lambda_2\simeq u_{i+1/2}+\sqrt{g(R_0h_{i+1/2}+\frac{\gamma_{i+1/2}}{2}+\frac{1}{2}(R_c)_{i+1/2}h_{i+1/2})},\tag{5.18b}$$

$$\lambda_{2+j}=u_{i+1/2},j=1,\cdots,n_s\ (\text{multiplicity } n_s),\tag{5.18c}$$

$$\lambda_{n_s+3}\simeq 0.\tag{5.18d}$$

As $R_0<0$, λ_1 and λ_2 may become complex when $\frac{1}{2}\gamma_{i+1/2}+\frac{1}{2}(R_c)_{i+1/2}h_{i+1/2}$ is small. Indeed, this situation may arise near the plume front or when most of the sediment has been deposited. In this situations the density of the turbidity current is lower than that of the ambient water an thus it should go upwards. Therefore, the model is no longer valid in such situations. Nevertheless, one would like to compute, for example, numerical simulations of dam-break type, where eigenvalues may become complex near the front but the model makes sense far from the front. One way to do so is to set $\rho_0=\rho_w$ if $\mathcal{A}_{i+1/2}$ has complex eigenvalues and to neglect the pressure terms. Thus, whenever $\mathcal{A}_{i+1/2}$ given by (5.10), (5.13a)-(5.13c) has complex eigenvalues, we replace locally the scheme by an upwinding method for the flux $\widetilde{F}$ without pressure terms. More explicitly, if the Roe matrix has complex eigenvalues at the inter-cell $x_{i_0+1/2}$, then the terms $\mathcal{A}^{\pm}_{i_0+1/2}(W_{i_0+1}-W_{i_0})$ in the scheme (5.7) are replaced by $D^{\pm}_{i_0+1/2}$ where

$$D^{-}_{i_0+1/2}=0,\quad D^{+}_{i_0+1/2}=\widetilde{F}^*(W_{i_0+1})-\widetilde{F}^*(W_{i_0})\quad \text{if } u_{i_0+1/2}>0, \tag{5.19a}$$

$$D^{-}_{i_0+1/2}=\widetilde{F}^*(W_{i_0+1})-\widetilde{F}^*(W_{i_0}),\quad D^{+}_{i_0+1/2}=0\quad \text{if } u_{i_0+1/2}<0, \tag{5.19b}$$

and

$$\widetilde{F}^*(W)=(hu,hu^2,hc_1u,\cdots,hc_{n_s}u,-\xi q_b)^t. \tag{5.20}$$

5.3 Addition of a non-erodible bed

Usually, the bottom is formed by a thin layer of sediments that may be eroded or transported by the plume that lays over a rigid bottom which is not erodible. In that case, an initial function $M_0(x)$ must be given that establishes the depth for the non-erodible bottom (see Fig. 2). Moreover, in some cases a fraction of the deposited sediment may solidify and become part of the non-erodible bottom so that M_0 could depend on time.

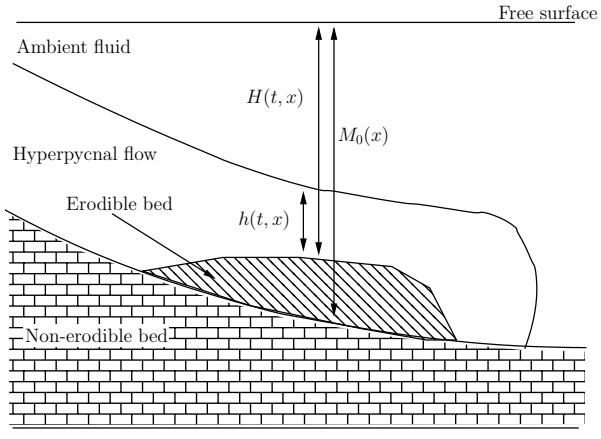

Figure 2: Sketch of hyperpycnal flow over a non erodible bed.

In this cases, the source terms $(\phi_b^j)^n = v_{s_j}(p_j^n E_{s_j}^n - c_{b_j}^n)$ have to be limited so that the amount of eroded sediment do not exceed the total mass of the erodible layer. Thus, for each cell I_i whenever $(\phi_b^j)^n > 0$, this source term is replaced by the modified expression

$$(\widehat{\phi}_b^j)^n = \begin{cases} (\phi_b^j)^n, & \text{if } p_j^n(M_0 - H^n) - \xi \triangle t (\phi_b^j)^n \geq 0, \\ p_j^n(M_0 - H^n)(\triangle t)^{-1}, & \text{otherwise.} \end{cases} \tag{5.21}$$

The volume fraction of sediments at the bottom, p_i^{n+1} is given by

$$p_j^{n+1}(M_0 - H^{n+1}) = p_j^n(M_0 - H^n) - \triangle t(\widehat{\phi}_b^j)^n \geq 0, \tag{5.22}$$

for each cell I_i. Note that (5.21) assures the positivity of p_j^{n+1}.

6 Extension to 2D

The model (2.14) can be easily extended to the 2D case. Following the same procedure of Section 3 adapted to the 2D case, one can obtain

$$\begin{cases} \partial_t h + \partial_x(hu) + \partial_y(hv) = \phi_\eta + \phi_b, \\ \partial_t(hu) + \partial_x\left(hu^2 + g(R_0+R_c)\dfrac{h^2}{2}\right) + \partial_y(huv) = g(R_0+R_c)h\partial_x H + u\phi_\eta + \dfrac{u}{2}\phi_b + \tau_u, \\ \partial_t(hv) + \partial_x(huv) + \partial_y\left(hv^2 + g(R_0+R_c)\dfrac{h^2}{2}\right) = g(R_0+R_c)h\partial_y H + v\phi_\eta + \dfrac{v}{2}\phi_b + \tau_v, \\ \partial_t(hc_j) + \partial_x(huc_j) + \partial_y(hvc_j) = \phi_b^j, \text{ for } j = 1, \cdots, n_s, \\ \partial_t H - \xi\partial_x q_b^x - \xi\partial_y q_b^y = \xi\phi_b, \end{cases} \tag{6.1}$$

where h is the current thickness; $\vec{u} = (u,v)$ is the depth-averaged velocity; c_j for $j = 1, \cdots, n_s$ represents the vertically averaged volume concentration of the jth sediment; and H is the bottom depth from a fixed level.

The expression of ϕ_η is now given by

$$\phi_\eta = E_w \|\vec{u}\|, \tag{6.2}$$

while the definition of ϕ_b^j remains essentially the same but replacing $|u|$ by $\|\vec{u}\|$ in (2.10). Let us denote

$$\tau_u = -(1+\alpha)c_D u\|\vec{u}\|, \quad \tau_v = -(1+\alpha)c_D v\|\vec{u}\|. \tag{6.3}$$

In the case of Grass model, (q_b^x, q_b^y) is the corresponding 2D solid transport flux which is given by

$$q_b^x = A_g u\|\vec{u}\|^{m_g - 1}, \quad q_b^y = A_g v\|\vec{u}\|^{m_g - 1}, \quad 1 \leq m_g \leq 4. \tag{6.4}$$

The system may be rewritten in the form:

$$\partial_t W+\partial_x \widetilde{F}_1(W)+\partial_y \widetilde{F}_2(W)=B_1(W)\partial_x W+B_2(W)\partial_y W+S(W), \tag{6.5}$$

where $W=[h,hu,hv,hc_1,\cdots,hc_{n_s},H]^t$ and

$$\widetilde{F}_1(W)=\left[hu,hu^2+g/2(R_0+R_c)h^2,huv,hc_1u,\cdots,hc_{n_s}u,-\xi q_b^x\right]^t, \tag{6.6a}$$

$$\widetilde{F}_2(W)=\left[hv,huv,hv^2+g/2(R_0+R_c)h^2,hc_1v,\cdots,hc_{n_s}v,-\xi q_b^y\right]^t, \tag{6.6b}$$

$$B_1(W)=g(R_0+R_c)he_{2,n_s+4}, \tag{6.6c}$$

$$B_2(W)=g(R_0+R_c)he_{3,n_s+4}, \tag{6.6d}$$

$$S(W)=\begin{pmatrix} E_w\|\vec{u}\|+\sum_{j=1}^{n_s} v_{s_j}(p_jE_{s_j}-c_{b_j}) \\ E_wu\|\vec{u}\|+\frac{u}{2}\sum_{j=1}^{n_s} v_{s_j}(p_jE_{s_j}-c_{b_j})-(1+\alpha)c_Du\|\vec{u}\| \\ E_wv\|\vec{u}\|+\frac{v}{2}\sum_{j=1}^{n_s} v_{s_j}(p_jE_{s_j}-c_{b_j})-(1+\alpha)c_Dv\|\vec{u}\| \\ v_{s_1}(p_1E_{s_1}-c_{b_1}) \\ \cdots \\ v_{s_{n_s}}(p_{n_s}E_{s_{n_s}}-c_{b_{n_s}}) \\ \xi\sum_{j=1}^{n_s} v_{s_j}(p_jE_{s_j}-c_{b_j}) \end{pmatrix}. \tag{6.6e}$$

Here $e_{r,s}=(\delta_{ir}\delta_{js})_{i=1,j=1}^{n_s+4,n_s+4}$ is the canonical basis of square matrices of order n_s+4.

The problem may also be written in the more general form

$$\partial_t W+\mathcal{A}_1(W)\partial_x W+\mathcal{A}_2(W)\partial_y W=S(W), \tag{6.7}$$

where $\mathcal{A}_k=\nabla\widetilde{F}_k(W)-B_k(W), \quad k=1,2.$

Some easy calculations allow us to prove the following property:

Lemma 6.1. *System* (6.1) *is invariant under rotations. More explicitly, suppose any unitary vector* $\vec{n}=(n_x,n_y)$ *and define*

$$R_{\vec{n}}=\left[\begin{array}{c|cc|c} 1 & 0 & 0 & 0 \\ \hline 0 & n_x & n_y & 0 \\ 0 & -n_y & n_x & 0 \\ \hline 0 & 0 & 0 & Id \end{array}\right]. \tag{6.8}$$

Then the following relations hold

$$\widetilde{F}_{\vec{n}}(W) := n_x \widetilde{F}_1(W) + n_y \widetilde{F}_2(W) = R_{\vec{n}}^{-1} \widetilde{F}_1(R_{\vec{n}} W), \tag{6.9}$$

$$B_{\vec{n}}(W) := n_x B_1(W) + n_y B_2(W) = R_{\vec{n}}^{-1} B_1(R_{\vec{n}} W) R_{\vec{n}}, \tag{6.10}$$

$$\mathcal{A}_{\vec{n}}(W) := n_x \mathcal{A}_1 + n_y \mathcal{A}_2 = R_{\vec{n}}^{-1} \mathcal{A}_1(R_{\vec{n}} W) R_{\vec{n}}. \tag{6.11}$$

In order to solve (6.7), the computational domain is divided into discretization cells or finite volumes, V_i and we proceed as it was done in Section 5 by solving first

$$\begin{cases} \partial_t W + \partial_x \widetilde{F}_1(W) + \partial_y \widetilde{F}_2(W) = B_1(W)\partial_x H + B_2(W)\partial_y H, \\ W(x,y,t=t^n) = W_i^n \text{ for } (x,y) \in V_i. \end{cases} \tag{6.12}$$

Then, let $W_i^{n+1/2}$ be the approximations of the cell averages of the solution of this problem. We define

$$W_i^{n+1} = W_i^{n+1/2} + \triangle t S(W_i^n). \tag{6.13}$$

Now, in order to write the Roe scheme, the following notation is considered: given a finite volume V_i, $\mathcal{N}_i$ is the set of indexes j such that V_j is a neighbor of V_i; E_{ij} is the common edge to two neighbor cells V_i and V_j, and $|E_{ij}|$ represents its length; and $\vec{n}_{ij} = (n_{ij,x}, n_{ij,y})$ is the normal unit vector of the edge E_{ij} pointing towards the cell V_j.

Following [7,8], the expression of the Roe scheme is now:

$$W_i^{n+1} = W_i^n - \frac{\triangle t}{|V_i|} \sum_{j \in \mathcal{N}_i} |E_{ij}| \mathcal{A}_{ij}^-(W_j^n - W_i^n), \tag{6.14}$$

where $\mathcal{A}_{i,j} = \mathcal{A}(W_i, W_j, \vec{n}_{ij})$ represents the Roe linearization of $n_x \mathcal{A}_1(W) + n_y \mathcal{A}_2(W)$. We refer to [7,8] for further details.

Thanks to Lemma 6.1, the definition of Roe matrices is an easy task by using the expression given for the 1D case. The eigenstructure of Roe matrix is also straightforward from Lemma 4.1.

7 Numerical simulations

7.1 A simple test case

We consider first a simple test to compare the conservation properties of systems (2.1) and (2.14). We consider a closed tank with flat topography. We suppose that the tank is initially filled with a mixture of water and some given sediment of density $2.65 g/cm^2$ and settling velocity $v_s = 0.1 m/s$. The initial concentration of the sediment is 0.07, the initial depth of the mixture is 0.1 and the initial velocity of the mixture is 0. It is clear that the sediment in the mixture will be deposed as time evolves until the experiment reaches a stationary solution where all sediment has been deposed at the bottom and we have clear water at rest over the topography.

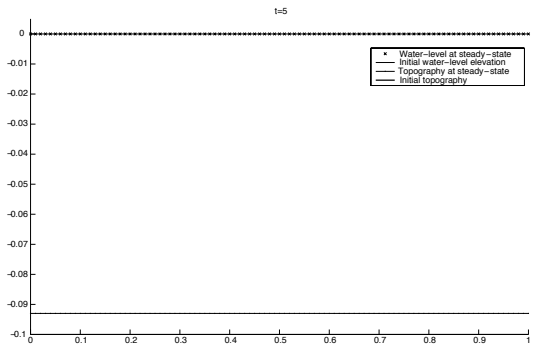

Figure 3: A simple test case: topography and water-level elevation at time $t=5$ given by (2.1).

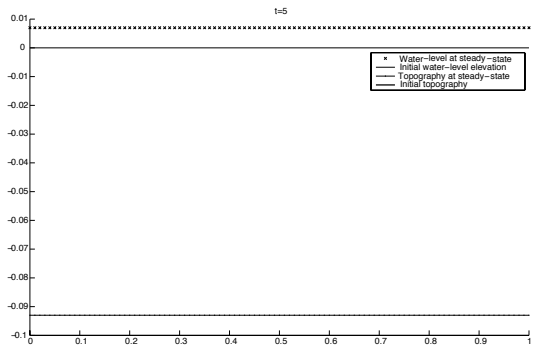

Figure 4: A simple test case: topography and water-level elevation at time $t=5$ given by (2.14).

Figs. 3 and 4 show the topography and water-level elevation of systems (2.1) and (2.14) respectively at time $t=5$, when all sediment has been deposed.

We remark that the freshwater mass is preserved by system (2.14) while it is not the case of system (2.1). Indeed, Fig. 4 shows that bottom topography at time $t=5$ is at level 0.093. This means that the water depth is equal to $0.093=0.1\cdot(1-0.7)$ and the sediment depth at the topography is equal to $0.007=0.1\cdot 0.07$. Thus, mass is preserved, which shows the relevance of additional source term in the first equation for system (2.14). The absence of this term in system (2.1) means that height h remains constant which makes that freshwater mass is increased by 7%

7.2 Comparison with laboratory experiments

Now, we compare the model with the data presented in [17] corresponding to a laboratory experiment using a 10-m-long, 0.2-m-wide and 0.5-m-deep flume with a 0.5-m-long gate box at the upstream end. Lock exchange experiments where studied with different bottom topographies and different sediment concentration at the gate box. For the experiment shown here, the initial water depth is 0.2 m at the gate box. The topography in the flume is given by Fig. 5.

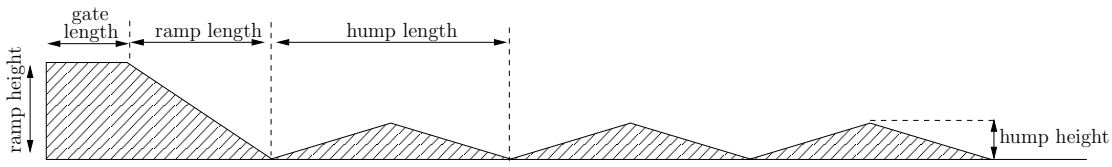

Figure 5: Comparison with laboratory experiments: Hump topography.

Particle-driven density currents were generated by releasing suspensions, which were composed by siliceous, non-cohesive, sand to silt sized particles (density $2650 kg/m^3$). The initial volume fraction of the particles was 2% and the solid transport of the bottom

is neglected ($q_b = 0$). The sediments are represented by a mixture of 20% of fine sand ($v_s = 0.01m/s$, $\phi = 3.0$), 50% very fine sand ($vs = 0.005m/s$, $\phi = 3.5$) and 30% of coarse silt ($vs = 0.003m/s$, $\phi = 4.0$).

We show the simulations corresponding to experiments B5, B9, B11, C5, C7 and C13 in [17]. The corresponding parameters for each experiment are given in Table 1.

Table 1: Experiment description.

Experiment	Ramp height	Ramp length	Number of humps	Hump height	Hump length
B5	0.1	1	0	-	-
B9	0.1	2	0	-	-
B11	0.05	1	0	-	-
C5	0.1	1	3	0.036	1
C7	0	1	3	0.036	1
C13	0.1	1	3	0.036	2

In general, the model predictions are comparable to the experimental results. In some cases, we remark that some disagreements arise, specially in the proximal area, where the model predicts less deposition than found in experimental results. This behaviour was also observed in the simulations shown in [17]. This is more likely due to the fact that the motion of the upper ambient layer has been neglected. When a turbidity current intrudes shallow water, an opposing current is generated in the ambient fluid, which reduces its forward momentum. In Fig. 6 we see that deposits decrease from a maximum at the beginning of the flume with a slight increase downstream of the slope break. This increase is sensible to the slope of the ramp. In the case of Fig. 7, the topography influence can be seen as an increase on upslope of the humps.

7.3 Successive turbidity currents over an initial flat bottom

Inspired by the experiments shown in [18], we intend now to simulate spillover turbidity currents on submarine channel levees, that is a succession over a long time period of several turbidity currents. Following this idea, we generate successive turbidity currents over an initial $25m$ long flat bottom. Each turbidity current is generated by supplying a suspension of sediments at the upstream end of the flow field. The mixture is composed by three sediment species with the same characteristics as the ones used on experiments given by Table 1. The height is fixed to $0.5m$ and the flux is $0.001m^2/s$. The supply duration is set at $4s$ and the turbidity is let to evolve for $100s$ before the next supply arrives. The volume of deposits is then converted to bed thickness so that the final bed after each supply is considered as the initial topography for the following and is supposed to solidify and to be non-erodible when the next plume arrives. In Fig. 8 we represent the bottom evolution for this successive flow events. Each layer represents the resulting bottom after 500 flow events. We remark the appearance of wavy structures by repeated deposition of turbidities over a flat bottom as it would be expected in physical situations.

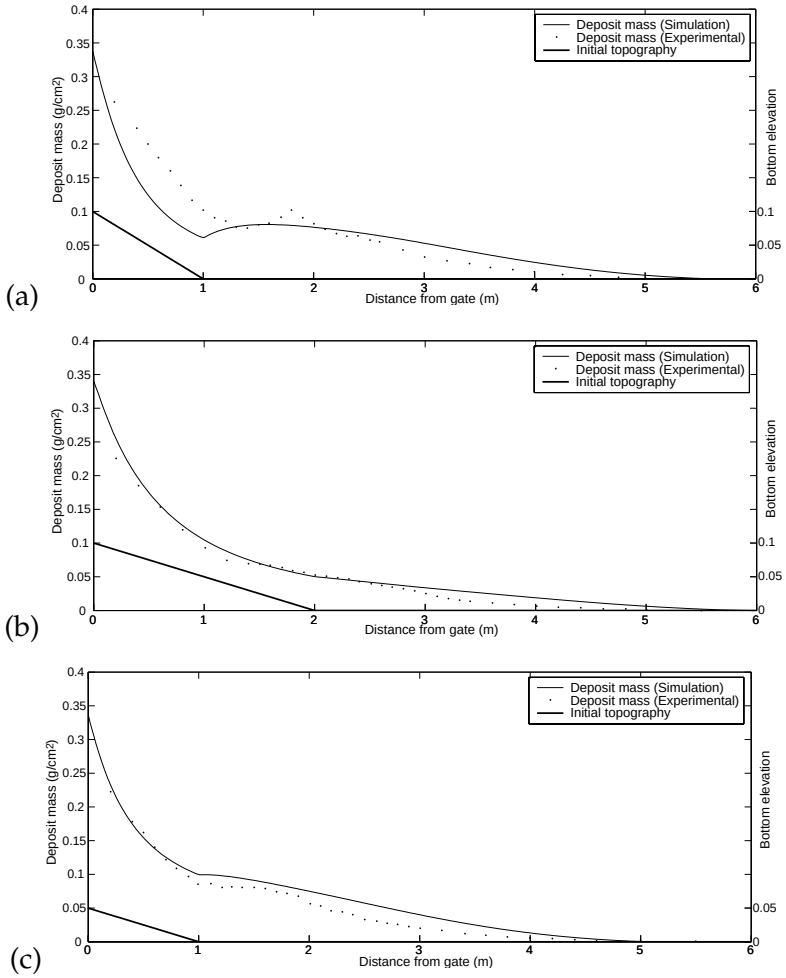

Figure 6: Comparison with laboratory experiments: Deposit distribution for experiments (a): B5, (b): B9, and (c): B11.

7.4 Solid transport of topography

We shall now show the influence of solid transport on the topography. We consider the case of a river (assume $R_0=0$) over an initial topography given by

$$H(x,t=0)=\begin{cases}0.1-0.04\sin^2(\pi(x-3)/2), & \text{for } 2\leq x\leq 5,\\ 0.1, & \text{elsewhere.}\end{cases} \tag{7.1}$$

This initial topography is assumed to be erodible up to the depth level 0.102. The initial height is set to $h(x,t=0)=H(x,0)$ and the initial velocity is such that $hu(x,t=0)=0.01$. We suppose that there is a suspension of siliceous particles (density $2650kg/m^3$ and $vs=0.002m/s$) with initial volume fraction of 1%. At the upstream end, we set a supply

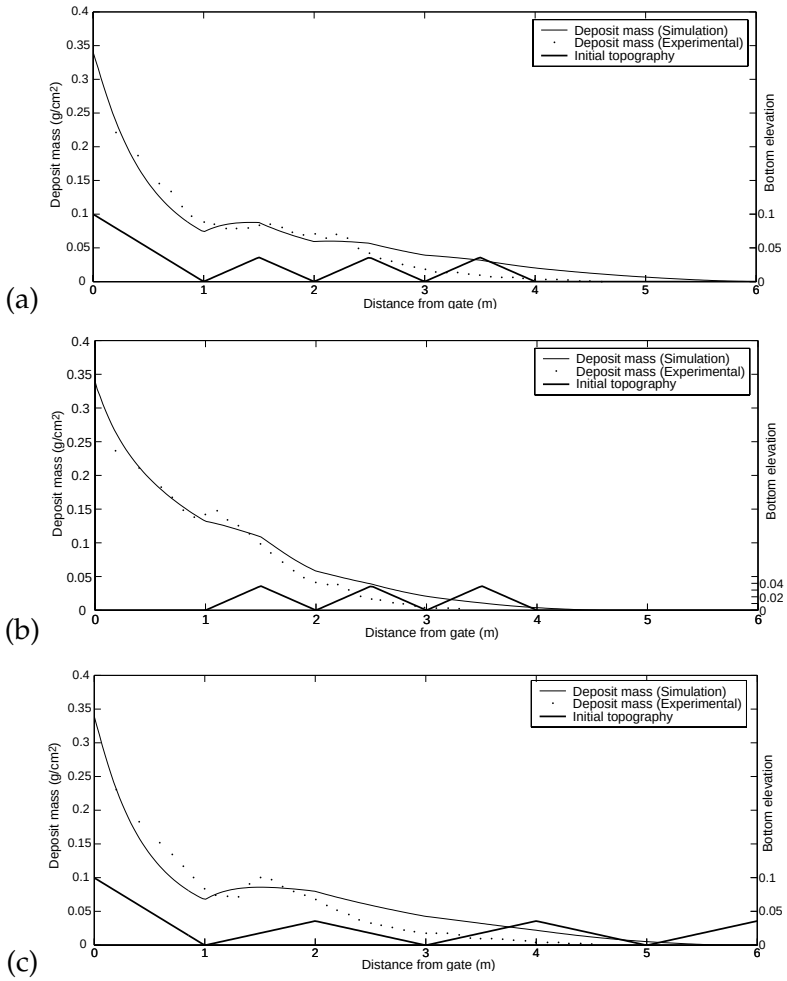

Figure 7: Comparison with laboratory experiments: Deposit distribution for experiments (a): C5, (b): C7, and (c): C13.

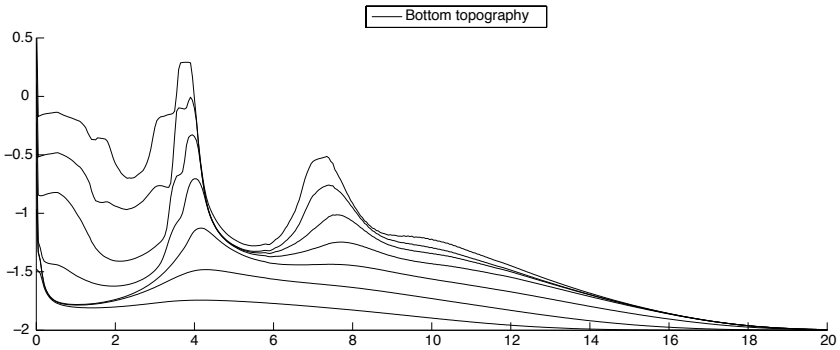

Figure 8: Successive turbidity currents over an initial flat bottom: Topography evolution. Each layer corresponds to 500 turbidity beds.

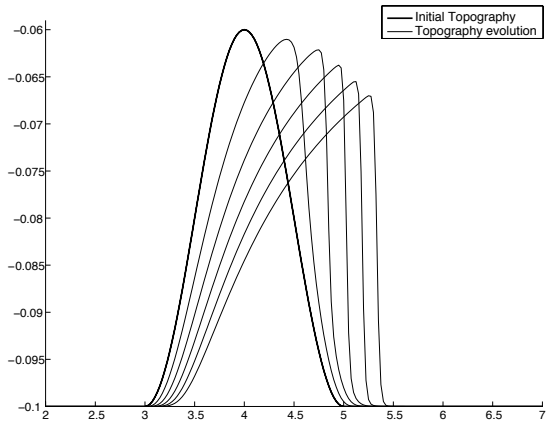

Figure 9: Solid transport of topography: Bottom evolution without erosion nor deposition of particles. Each layer represents $400s$.

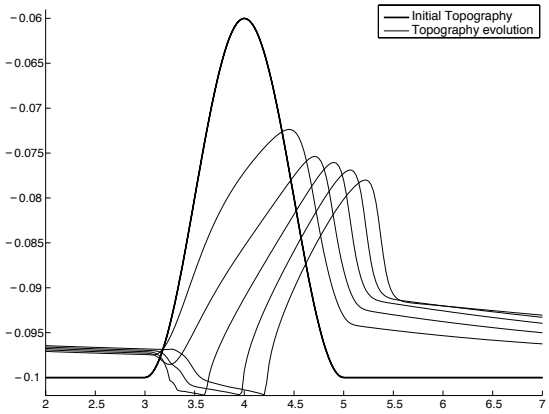

Figure 10: Solid transport of topography: Bottom evolution with erosion and deposition of particles. Each layer represents $400s$.

with concentration 1% for the first $100s$. Solid transport is considered using Grass model with $A_g = 0.005$.

First, assume that there is no erosion of the topography and no deposition of particles, so that only solid transport is considered. Fig. 9 shows the topography evolution.

Now, let us consider the same situation but adding erosion and deposition effects. The results are shown on Fig. 10.

7.5 A 2D example

We consider here a 2d test related to experiment C5 in Section 7.2. We consider the domain given by Fig. 11. A 0.5-m-long by 1-m-wide gate box has been placed at the up-

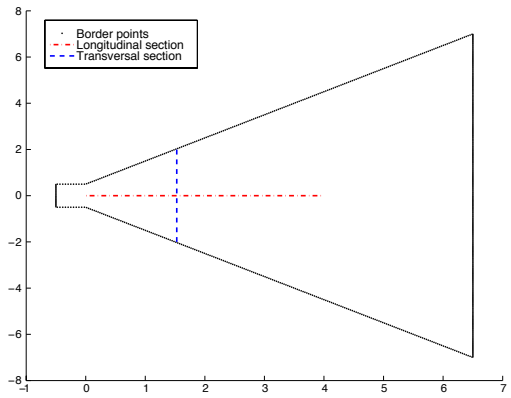

Figure 11: A 2D example: Domain and sections.

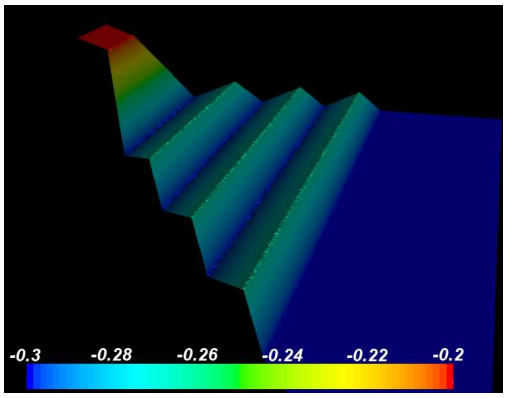

Figure 12: A 2D example: Bottom depth.

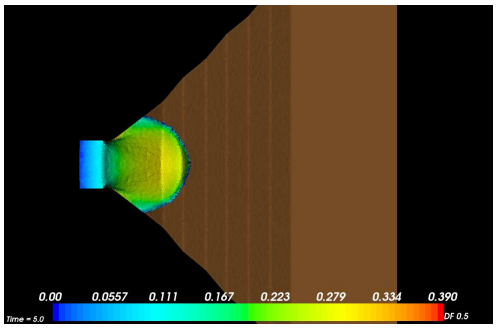

(a)

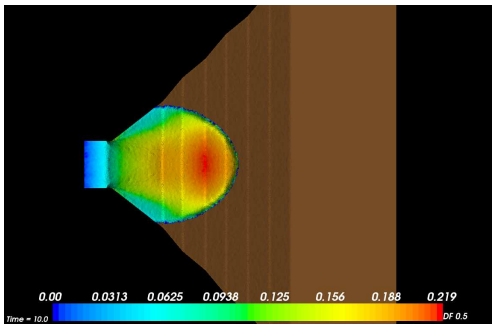

(b)

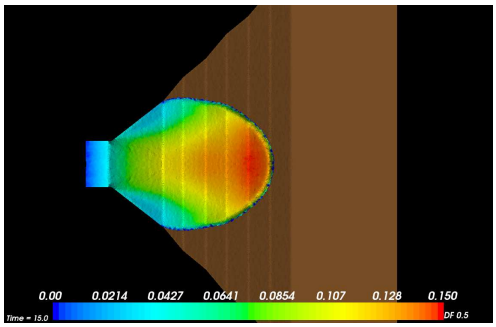

(c)

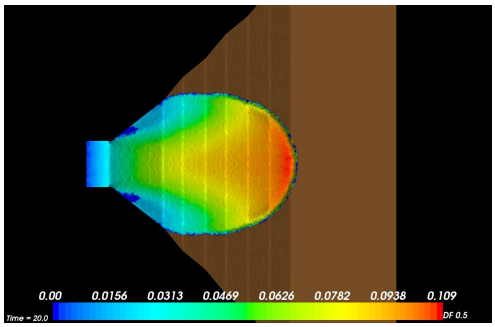

(d)

Figure 13: A 2D example: Evolution of turbidity current after release from the gate box. Color levels correspond to the modulus of velocity.

stream end with a mixture of sediments with same characteristics as the ones used in Section 7.2. The initial height of the mixture is set to 0.2m and we consider a hump topography like the one on Fig. 12 with ramp and hump height and length corresponding to experiment C5 in Section 7.2.

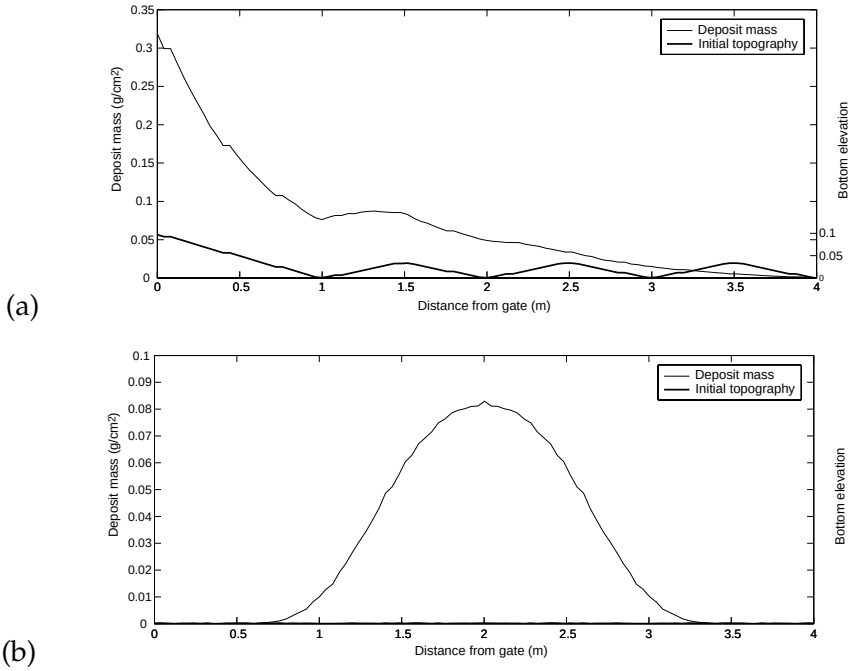

Figure 14: A 2D example: Deposit density. (a): Longitudinal section, (b): Transversal section.

Fig. 14 shows the deposit density along the longitudinal and transversal sections on Fig. 11.

Acknowledgments

This research has been partially supported by the Spanish Government Research projects MTM2006-08075 and P06-RNM-01594. The numerical computations have been performed at the Laboratory of Numerical Methods of the University of Málaga.

References

[1] J. Alexander and S. Morris. Observations on experimental, nonchannelized, high-concentration turbidity currents and variations in deposits around obstacles. Journal of Sedimentary Research, 64:899–909, Oct. 1994.

[2] M. Altinaker, W. Graf, and E. Hopfinger. Flow structure in turbidity currents. Journal of Hydraulic Research, 34(5), 1996.

[3] F. Bouchut, E. Fernández-Nieto, A. Mangeney, and P.-Y. Lagrée. On new erosion models of savage-hutter type for avalanches. Acta Mechanica, 199:181–208, 2008.

[4] F. Bouchut, A. Mangeney-Castelnau, B. Perthame, and J.-P. Vilotte. A new model of Saint Venant and Savage-Hutter type for gravity driven shallow water flows. C. R. Math. Acad. Sci. Paris, 336(6):531–536, 2003.

[5] F. Bouchut and M. Westdickenberg. Gravity driven shallow water models for arbitrary topography. Comm. Math. Sci., 2(3):359–389, 2004.
[6] S. F. Bradford and N. D. Katopodes. Hydrodynamics of turbid underflows. i: Formulation and numerical analysis. Journal of Hydraulic Engineering, 125(10):1006–1015, 1999.
[7] M. Castro, E. Fernández-Nieto, A. Ferreiro, J. García-Rodríguez, and C. Parés. High order extensions of roe schemes for two-dimensional nonconservative hyperbolic systems. Journal of Scientific Computing, 39(1):67–114, 2009.
[8] M. J. Castro, J. A. García-Rodríguez, J. M. González-Vida, and C. Parés. A parallel 2d finite volume scheme for solving systems of balance laws with nonconservative products: application to shallow flows. Comput. Methods Appl. Mech. Engrg., 195(19-22):2788–2815, 2006.
[9] F. H. Chu, W. D. Pilkey, and O. H. Pilkey. An analytical study of turbidity current steady flow. Marine Geology, 33(3-4):205–220, 1979. Cited By (since 1996): 11.
[10] G. Dal Maso, P. G. Lefloch, and F. Murat. Definition and weak stability of nonconservative products. J. Math. Pures Appl. (9), 74(6):483–548, 1995.
[11] W. Dietrich. Settling velocities of natural particles. Water Resources Research, 18(6):1615–1626, 1982.
[12] M. Garcia and G. Parker. Experiments on the entrainment of sediment into suspension by a dense bottom current. Journal of Geophysical Research, 98(C3):4793–4808, 1993.
[13] M. H. García. Hydraulic jumps in sediment-driven bottom currents. Journal of Hydraulic Engineering, 119(10):1094–1117, 1993.
[14] A. Grass. Sediment transport by waves and currents. SERC London Cent. Mar. Technol, Report No. FL29, 1981.
[15] J. M. Gray. Granular flow in partially filled slowly rotating drums. J. Fluid Mech., 441:1–29, 2001.
[16] S. M. Khan, J. Imran, S. Bradford, and J. Syvitski. Numerical modeling of hyperpycnal plume. Marine Geology, 222-223:193–211, 2005.
[17] Y. Kubo. Experimental and numerical study of topographic effects on deposition from two-dimensional, particle-driven density currents. Sedimentary Geology, 164(3-4):311–326, 2004.
[18] Y. Kubo and T. Nakajima. Laboratory experiments and numerical simulation of sediment-wave formation by turbidity currents. Marine Geology, 192(1-3):105–121, 2002.
[19] E. Meyer-Peter and R. Müller. Formulas for bed-load transport. In 2nd meeting IAHSR, Stockholm, Sweden, pages 1–26, 1948.
[20] G. V. Middleton. Experiments on density and turbidity currents: III. Deposition of sediment. Canadian Journal of Earth Sciences, 4:297–307, 1967.
[21] P. Nielsen. Coastal Bottom Boundary Layers and Sediment Transport. World Scientific, 1992.
[22] C. Parés. Numerical methods for nonconservative hyperbolic systems: a theoretical framework. SIAM J. Numer. Anal., 44(1):300–321 (electronic), 2006.
[23] C. Parés and M. Castro. On the well-balance property of Roe's method for nonconservative hyperbolic systems. Applications to shallow-water systems. M2AN Math. Model. Numer. Anal., 38(5):821–852, 2004.
[24] G. Parker, Y. Fukushima, and H. M. Pantin. Self-accelerating turbidity currents. J. Fluid Mech., 171:145–181, 1986.
[25] I. Toumi. A weak formulation of Roe's approximate Riemann solver. J. Comput. Phys., 102(2):360–373, 1992.